ESTIMATION OF THICKNESS AND LAYERING OF JOHANSEN AND COOK SANDSTONES AT THE POTENTIAL CO_2 STORAGE SITE AURORA

Eyvind Aker[1*], Heidi Kjønsberg[1], Manzar Fawad[2], Nazmul Haque Mondol[2,3]

[1] Norwegian Computing Center, Oslo, Norway

[2] Institute of Geology, University of Oslo, Oslo, Norway

[3] Norwegian Geotechnical Institute, Oslo, Norway

* Corresponding author e-mail: eyvind.aker@nr.no

Abstract

We have estimated the reservoir sand thickness and internal layering in the Aurora area, a planned geological CO_2 storage site in the northern North Sea. The results are obtained by stochastic Markov chain Monte Carlo (MCMC) simulations on probabilistic lithology and fluid distributions in the subsurface. The probabilistic distributions are obtained by inverting the seismic data in a Bayesian framework. The inversion is using angle-dependent pre-stack seismic data and the linearized seismic forward model of Aki and Richards to estimate the posterior probabilities of lithology and fluid classes (facies) in the subsurface. The facies are defined from well log data by identifying depth intervals with distinct elastic responses to seismic waves. The inversion methodology and the MCMC simulations are developed and implemented by the Norwegian Computing Center.

The planned CO_2 storage reservoir comprises the Johansen and Cook sandstones belonging to the Early Jurassic Dunlin Group. The injection site (well 31/5-7) is located south and west of the Troll field in the northern North Sea and is currently being developed by Equinor in partnership with Total and Shell as part of the Northern Light project.

The seismic inversion is mapping structural details like faults and internal layering of the sandstones, and the MCMC simulations estimate the probability of sand thickness and expected layering. Results show that the Johansen Formation sandstone has a tendency of layering towards the west and largest thickness to the east in the inversion area. The sandstone in the Cook Formation is generally thinner, and probability maps indicate that it pinches out to the east. Cumulative thickness distributions provide low (P90), median (P50), and high (P10) thickness maps of both Johansen and Cook Formation sandstones. The presented methodology defines a functional workflow for quantifying the thickness uncertainty and possibly internal layering of the reservoir sands. Such results may provide important input for future field development strategies and CO_2 migration predictions.

Keywords: *CO_2 storage, Aurora, Cook and Johansen Formation, Seismic inversion, Bayesian probability, Markov chain Monte Carlo simulations*

1. Introduction

In hydrocarbon exploration, seismic data is used for mapping potential hydrocarbon accumulations below the seabed, with subsequent drilling of wildcat and appraisal wells to prove the reserves. Similar operations are expected in the exploration phase of a CO_2 storage project. However, we may expect fewer wells and less adequate seismic data coverage than what is typical in a hydrocarbon project since the economic viability of injecting CO_2 is lower than corresponding oil and gas production. Less data would often lead to higher uncertainty about the storage reservoir properties. Therefore, methodologies that can lower and quantify the uncertainty from data would be valuable.

Seismic inversion is the process of transforming seismic reflection data to quantitative knowledge of the subsurface, often represented by rock properties. The inversion is routinely being performed by geophysicists gathering knowledge of hydrocarbon reservoirs in the exploration and production phase. In recent years, inversion methodologies for probabilistic lithology and fluid predictions have been developed, e.g. [1-6]. These techniques are using a Bayesian statistical framework suitable for lowering the uncertainty of an initial belief by observing (relevant) data. More specifically, the Bayesian seismic inversion methods seek to estimate a posterior probability model of different facies in the subsurface, based on a prior probability model and the seismic data. The facies can be defined as bodies of rock and fluid with varying distributions of elastic properties. For better facies predictions, the Bayesian methods utilize angle-dependent information and the inversion engine's forward model is often based on the Aki and Richards approximation [7] of the seismic amplitude variations with offset (AVO).

The layered structure of geological formations makes them suitable for modeling in terms of Markov chains [8], where the properties in one location depend only on the properties in the neighbor locations. Vertical continuities and transitions between facies layers can be described by transition probabilities that encompass a Markov chain model. Strict ordering of facies based on

for example geologic knowledge of the deposition can be accounted for. Various models like single trace [1], extensions to 3D [9-10], and more general Markov random field models [11-12] have been investigated in recent years.

We use a Bayesian-based AVO inversion process that is developed by the Norwegian Computing Center to invert a 3D seismic cube within the Aurora area. The inversion model estimates the probability of different facies combinations within a short window centered around every sample point [6]. The probabilities are used to construct a 1D Markov model to estimate the marginal probabilities of each facies class in every sample and to simulate realizations of the subsurface using Markov chain Monte Carlo simulations. From the realizations, we estimate distributions of thicknesses and probability of the presence of Johansen and Cook sandstones for every trace in the inversion area. The results are presented in probability cubes, maps of thickness estimates, and the accumulated probability of presence. The latter is interpreted as the expected number of internal layers of the sands. All results are shown for both Johansen and Cook sandstones.

2. Geological setting

The northern North Sea has undergone two main rifting events, which took place during Permo-Triassic and the Late Jurassic to Mid-Cretaceous times [13-14]. A wide basin with deep-rooted faults and thick syn-depositional wedges established below the Horda Platform during the first rifting event. The major rifting and tilting shifted westward (i.e., Lomre Terrace) during Late Jurassic to Mid Cretaceous event [15]. A weak stretching continued with the reactivation of major Permo-Triassic faults on the Horda Platform. The large normal faults with predominant N, NE and NW orientations mainly controlled the basins with several kilometres of throw-bound half grabens (15-50 km in width) and are the rifted area's fundamental morphological elements (Figure 1).

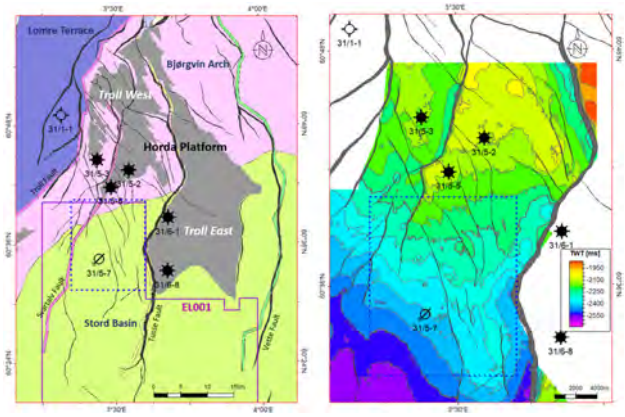

Figure 1: Inversion area (blue dotted rectangle) with the location of injection (31/5-7) and exploration wells. Well 31/5-7 was drilled within the exploitation license (EL001) for CO_2 storage (left). The colored map is a two-way time (TWT) surface of the top Johansen Formation (right).

A general stratigraphic section of the area is shown in Figure 2. The potential CO_2 storage reservoir comprises brine-filled sandstones in Johansen and Cook Formations belonging to the early Jurassic Dunlin Group. The Johansen Formation consists of sandstones with thin calcite cemented streaks [18]. The lower part is medium- to fine-grained, micaceous, well-sorted sandstone, which grades downwards into light grey silty micaceous claystone. The uppermost part is composed of medium- to fine-grained, micaceous sandstones, which are moderately sorted, silty, and argillaceous [19]. The Cook Formation consists of very fine to fine-grained, subangular to subrounded, well-sorted, hard to friable sandstones [18]. Mica, glauconite, carbonaceous material, and calcareous cement are present. Shales and siltstones separate the Johansen and Cook Formations, but they can be treated as one reservoir due to fault juxtaposition.

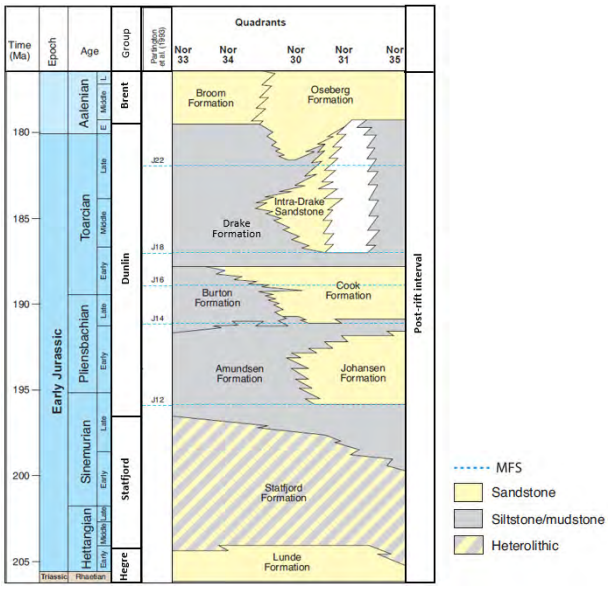

Figure 2: A generalized Early Jurassic stratigraphic succession of the study area (modified from [16]). MFS is the maximum flooding surface, according to [17].

The storage reservoirs and overlying caprocks were deposited after the Permo-Triassic rifting. The reservoir sandstones of Johansen Formation are prograding and retrograding deltaic in nature deposited during a lowstand [20]. The Amundsen Formation mudstones, which interfinger the Johansen Formation, consist of light to dark grey, non-calcareous siltstones and shales, in part carbonaceous and pyritic. The reservoir sandstone of Cook Formation is represented by prograding shelf sand on the Horda Platform and along its western margin [19]. The primary seal, i.e., Drake Formation, overlies the Cook Formation sandstone in most of the area; however, it directly overlies the Johansen Formation where the Cook and Amundsen Formations pinch out. The Drake Formation consists of medium grey, slightly sandy, calcareous, and silty claystone. The upper section is dark grey to black, fissile, micaceous shale containing calcareous nodules. Some fine to coarse sandstones are present in the formation within the study area [19].

3. Data

3.1 Geophysical data

We extracted small partial-stack cubes from the original GN10M1 seismic survey for inversion (Figure 1). The 3D seismic data is mostly of good quality, having been acquired reasonably recently in 2010. The partial stack cubes comprised angles 0-10°, 10-20°, 20-30°, and 30-40°. The inline and crossline intervals were 25 m and 12.5 m, respectively, whereas the vertical sampling rate was 4 ms. Statistical wavelets from all the five partial stacks were extracted using the entire volumes keeping the wavelet length of 200 ms. Wells 31/5-2 and 31/5-7 were correlated with the post-stack (GN10M1) seismic using sonic and checkshot data. A peak in the seismic trace represented a hard event. The interpretation of horizons was carried out based on the interface characteristics, i.e., hard or soft event, by selecting peak or trough accordingly. The horizon interpretation was initially carried out using the wells as control points, and then the 3D seeded autotracking was employed to fill the gaps. A relatively small cube surrounding the injection well is chosen for the inversion to save computational time and to get fast-track results. The injected CO_2 is expected to migrate towards north to the Troll West field and follow the updip layers of the reservoir sandstones.

3.2 Well data

The well database comprises seven exploration wells, as displayed in the map of Figure 1. Well 31/5-7 that is inside the inversion area was completed in early 2020 and is proposed as the CO_2 injection well of the Aurora license. Wells 31/1-1, 31/5-7, 31/5-2, and 31/6-1 penetrate the Johansen Formation and have been used to define the elastic properties of the facies in the inversion (see section 5). Gamma ray log, P- and S-wave velocity (V_p and V_s) and density (ρ) logs were obtained from the Norwegian National Data Repository for Petroleum Data (DISKOS), and formation well tops were downloaded from the Norwegian Petroleum Directorate fact-pages [19].

4. Methodology

We use the Bayesian AVO inversion methodology that is developed by the Norwegian Computing Center [6]. The method is inverting angle-dependent pre-stack seismic data to facies classes in a Bayesian framework. It estimates the posterior probabilities of the facies from a prior probability model and a data likelihood model quantifying how probable it is to observe the seismic data given combinations of facies in the subsurface.

In the following, facies should be thought of as a body of rock and fluid that causes a seismic response in the data and is characterized by a certain distribution of elastic properties. The distribution is represented by the mean and covariance of V_p, V_s, and ρ.

Let the seismic angle gather at a specific lateral location be denoted as $\mathbf{d}$, corresponding to an assumed response of a vertical column (trace) of facies $\mathbf{f}$ in the subsurface. Then Bayes' rule states that the posterior probability distribution of facies given the seismic data, $p(\mathbf{f}|\mathbf{d})$, is expressed by

$$p(\mathbf{f}|\mathbf{d}) = \frac{p(\mathbf{d}|\mathbf{f})p(\mathbf{f})}{p(\mathbf{d})}$$

Here $p(\mathbf{d}|\mathbf{f})$ is the data likelihood model, $p(\mathbf{f})$ is the prior probability model for facies distribution, and $p(\mathbf{d})$ is the probability distribution of observing the data.

In practice, we do not compute the full distribution of $p(\mathbf{d}|\mathbf{f})$ because the number of different facies combinations along the trace is far too high to be manageable. Instead, we assume that $p(\mathbf{d}|\mathbf{f})$ can be approximated in a neighborhood around each location and define the neighborhood to be a short vertical window of typically three to five samples. If for example, three different facies can exist at a specific location in the trace, then a five-sample length window centered around the location will result in $3^5 = 243$ different facies combinations. Hence, the problem is reduced to compare the expected seismic of these 243 different combinations (windows) with the recorded data. When there is a good match, the likelihood of the seismic data becomes high and vice versa.

By sliding the windows downwards along the trace, an approximate posterior probability of each window, $p_*(\mathbf{f}_w|\mathbf{d})$ is computed at every sample. The procedure is repeated for every lateral trace location in the seismic cube. The prior model $p(\mathbf{f}_w)$ as well as the approximate likelihood $p_*(\mathbf{d}|\mathbf{f}_w)$ utilize vertical Markov chains to account for spatial continuity and transitions among facies. See [6] for further details on how to compute $p_*(\mathbf{f}_w|\mathbf{d})$ and the resulting approximate marginal posterior probability for facies in every sample.

The expected seismic of the windows is computed by using the seismic forward model defined in [21]. It is a convolutional model based on the linearized approximation of the Aki and Richards equations [7] with added frequency-dependent Gaussian noise.

Note that the facies combinations of the windows entail the inversion to specifically look for reflections caused by facies transitions or thin layers. Layer thicknesses down to one sample are checked, despite being thinner than the seismic tuning thickness.

4.1 Creation of the posterior Markov chain

To extract additional outputs from the inversion like expected thickness and probability of the presence of individual facies, we create a posterior Markov model. It is constructed by taking the approximate window posterior probabilities $p_*(\mathbf{f}_w|\mathbf{d})$ and compute the posterior transition probabilities between facies at every sample along the trace. The vertical resolution of the Markov model is the seismic sample rate, and the calculations are repeated for every lateral location.

For facies that can disappear and re-enter further down the trace, we must sample from the posterior Markov model to get informative results. The sampling is performed by using Markov chain Monte Carlo simulations, and the number of simulations is typically

several 1000s depending on the complexity of the model. From the simulations, we can estimate distributions of thickness and probability of presence for individual facies. The latter is summed in the vertical direction and can be interpreted as the expected number of distinct layers. From the thickness distributions, we estimate the cumulative thickness generating low (P90), median (P50), and high (P10) thickness maps.

5. Litho-fluid classification

The different facies are classified by using the gamma ray log as an indicator for shale/sand content, well tops as an indicator for zonation between different depositional settings, and elastic logs (V_p, V_s, and ρ) for identifying depth intervals of distinct seismic responses.

Figures 3 and 4 show the facies classification obtained from the well logs of 31/1-1 and 31/5-7, focusing on the sands and shales in and around the Johansen and Cook Formations. The plotted depth is the measured depth with reference to the drill deck (Kelly bushing), and the horizontal dashed lines are the interpreted formation tops. The top names are shown in the yellow column. The log tracks from left to right is displaying ρ in units of g/cm^3, gamma-ray (GR) in unit API, acoustic impedance (AI) in unit of km/s·g/cm^3 and V_p/V_s (unitless). The last column shows the facies' classification in different colors, where white is unclassified/not used.

The well log data can be classified into six facies. The facies "Johansen sandstone" and "Cook sandstone" comprise the sandy parts of the Johansen and Cook Formations. "Dunlin shale" represents the shalier sediments in the Dunlin group, while "Drake shale" seems to only appear in the Drake Formation with a slightly higher V_p/V_s (see Figure 4). In the Statfjord Formation, there are intervals with higher V_p/V_s ratio than "Dunlin shale" and higher AI than "Drake shale". These intervals constitute the "Statfjord" facies. The AI logs in Figures 3 and 4 contain characteristic spikes that could be caused by thin layers of hard calcareous cemented shale and/or sandstone. They form the basis for the "Stringer" facies class.

The distribution of elastic properties of the six facies is inferred from the recorded V_p, V_s, and ρ of the classified points in Figures 3 and 4. The result is displayed in Figure 5 cross-plotting V_p/V_s versus AI. The variance of the distributions is manually lowered to compensate for the upscaling effect from well logs to seismic data. Moreover, the distributions define the probability distributions of elastic properties in the forward model of the inversion. Since both Johansen and Cook Formations are brine-saturated, it is not necessary to consider fluid effects (like oil and gas) on the elastic properties.

The recorded V_p and ρ in wells 31/5-2 and 31/6-1 overlap reasonably well with the facies classification in Figure 4 and the resulting elastic distributions in Figure 5. Thus, we assume that the estimated distributions can characterize the rock in the entire inversion area. Note that V_s was only recorded in wells 31/1-1 and 31/5-7; therefore, lateral variability of those values is uncertain.

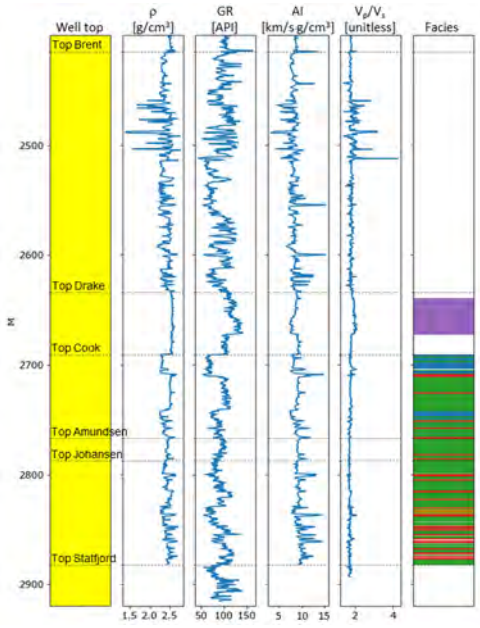

Figure 3: Facies classification in well 31/1-1.

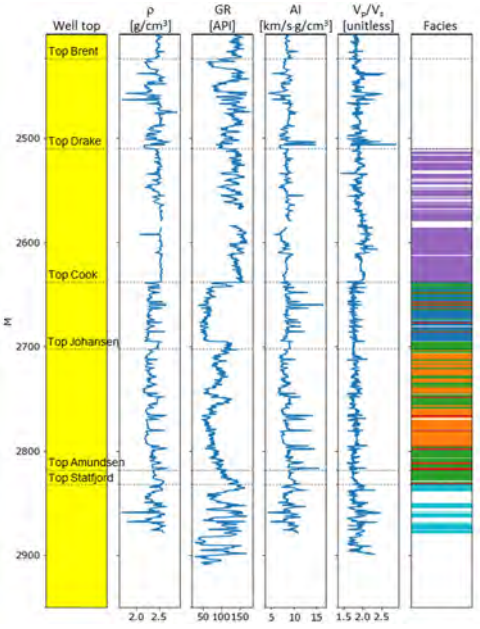

Figure 4: Facies classification in well 31/5-7.

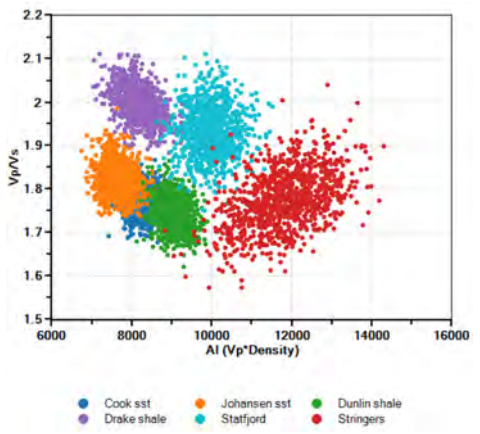

Figure 5: Elastic distributions of the facies.

6. Inversion

6.1 Prior probability model

The facies' prior probability model is constructed by a Markov chain, and the resulting model along a single trace is shown in Figure 6. The model comprises of the interpreted horizons Drake 2, Cook 4, Johansen 4, and Statfjord dividing the inversion interval into five zones from top to bottom. An initial uncertainty of +/- 10 ms is applied to the depth (time) of the interpreted horizons.

The prior probabilities of the facies and their expected thicknesses within each zone are defined from our initial belief and are based on the interpretation of well log data and the geological background knowledge. The prior input values are listed in Table 1, where the thickness values define the probability of staying in a facies class. We let the probability for transitions between different facies be evenly distributed within each zone.

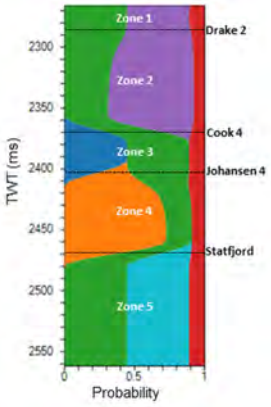

Figure 6: Prior probability model along a single trace.

The inversion interval is 300 ms and starts 20 ms above Drake 2 (zone 1) and stops in Statfjord (zone 5). The total number of traces in the inversion area is 755,970, and the number of facies combinations in the window is 648 with a window length of three samples. We do not assume any apriori ordering of the faces within a zone and allow vertical transitions between all facies with non-zero probability. The computation time of the inversion was about 40 minutes on a Windows computer with 24-core 3.0 GHz processor and 128 GB ram.

Elastic properties of the inverted result are inferred from the marginal posterior probability of facies and their corresponding elastic distribution mean values. The result is compared with the elastic logs at 31/5-7, giving a reasonable match and the inversion model seems to confirm the observations in the well.

Zone	Cook sst	Johan-sen sst	Dunlin shale	Drake shale	Stat-fjord	Stringers
1	0	0	0.45 / 20 ms	0.45 / 20 ms	0	0.1 / 5 ms
2	0	0	0.45 / 20 ms	0.45 / 40 ms	0	0.1 / 5 ms
3	0.45 / 20 ms	0	0.45 / 20 ms	0	0	0.1 / 5 ms
4	0	0.45 / 40 ms	0.45 / 10 ms	0	0	0.1 / 5 ms
5	0	0	0.45 / 20 ms	0	0.45 / 20 ms	0.1 / 5 ms

Table 1: Prior probabilities of each facies. Prior thickness is given in time (ms) for facies with non-zero prior probabilities. Listed probabilities refer to values at the top of each zone.

6.2 Posterior results

Figure 7 shows the posterior probability of Johansen sandstone within the Johansen Formation along cross-sections A-A' and B-B' intersecting well 31/5-7 (Figure 8). The posterior probability of sand appears high (close to 1) immediately below top Johansen 4 in both cross-sections. A solid thick interval with probability close to 1 from top to bottom of the Johansen formation is observed east of the well in section A-A'. The probability tends to drop or split between a lower and an upper peak west and south of the well in cross-sections A-A' and B-B', respectively.

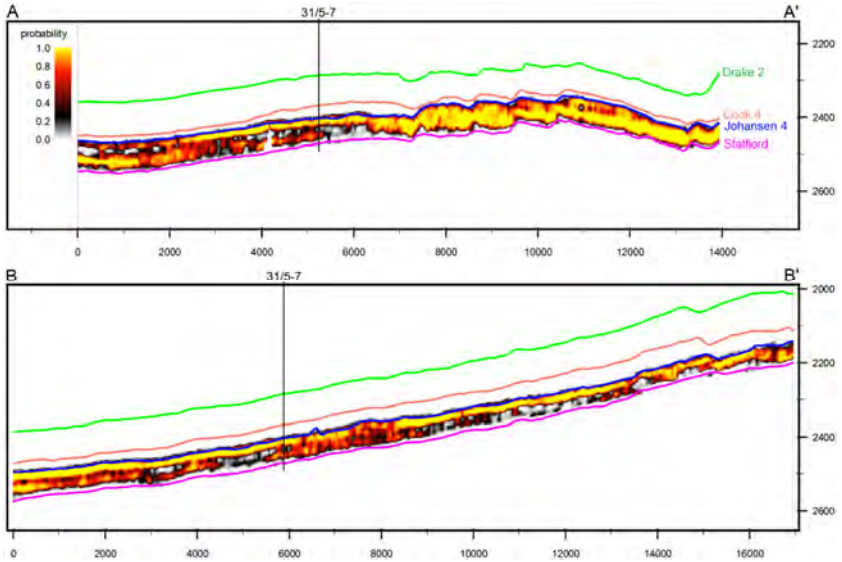

Figure 7: Posterior probability of Johansen sandstone along cross-sections A-A' and B-B' (see Figure 8). Solid colored lines correspond to the interpreted horizons.

The thickness distribution of the Johansen sandstone is estimated from MCMC simulations using the posterior Markov model. Five thousand realizations were simulated, and the resulting expected (mean) thickness is shown in Figure 8. The colors in the map span from 0 to 60 ms thickness. The thickness (in meters) is approximately double these numbers according to the time to depth conversion of well 31/5-7.

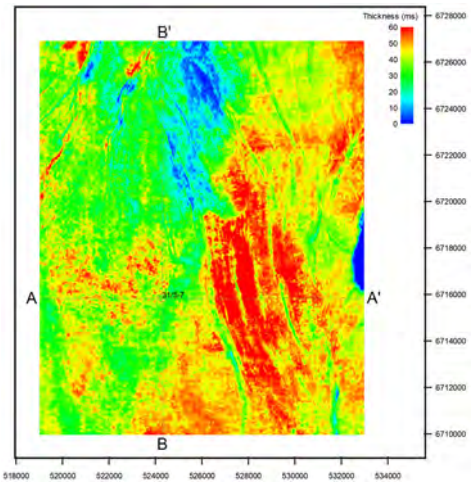

Figure 8: Expected thickness of the Johansen sandstone with well 31/5-7 and cross-sections overlaid.

The Johansen sandstone seems to be generally thickest to the east with a maximum expected thickness above 60 ms. Towards west and north, the thickness is lower and about 30 ms at the well 31/5-7. Notice the NNW-SSE sinusoidal shaped features of lower thickness to the east. They correspond to faults in the area, and the largest ones are also seen as four characteristic steps in the posterior probability in Figure 7 at around 7500, 8500, 9500, and 10500 meters in cross-section A-A'. Similar features were reported in [22].

The Johansen sandstone can disappear and reappear further down in the Johansen Formation, and the posterior probability in Figure 7 indicates that the sand may have some internal layering. To quantify the degree of layering, we let the vertical sum of probability of presence correspond to the expected number of layers. The result is plotted in Figure 9 for the Johansen sandstone.. Zero means that the Johansen sandstone is not present. The figure shows that there is a tendency for the sand to split into more than one layer as we move towards the west. There is also a small region towards the north where the probability of presence is very low and close to zero. The observed layering is confirmed by horizon interpretation from the seismic data identifying an internal horizon inside the Johansen formation.

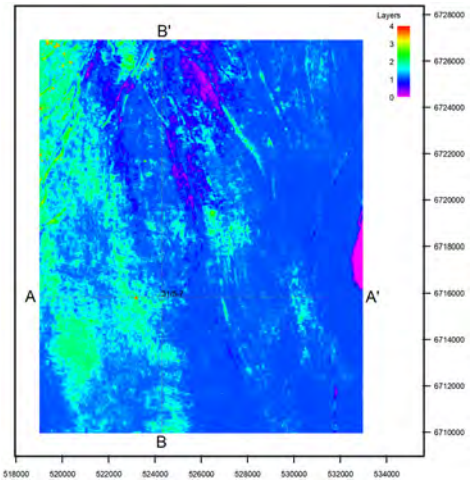

Figure 9: Expected number of layers of Johansen sandstone.

Figure 10 shows the cross-sections A-A' and B-B' for the posterior probability of Cook sandstone in the Cook Formation. The estimated probability of Cook sandstone is generally lower than the corresponding probability of Johansen sandstone (Figure 7). This is presumably because the elastic distribution of Cook sandstone is partly overlapped by Dunlin shale (see Figure 5), making them elastically more similar than the Johansen sandstone and more difficult for the inversion to resolve.

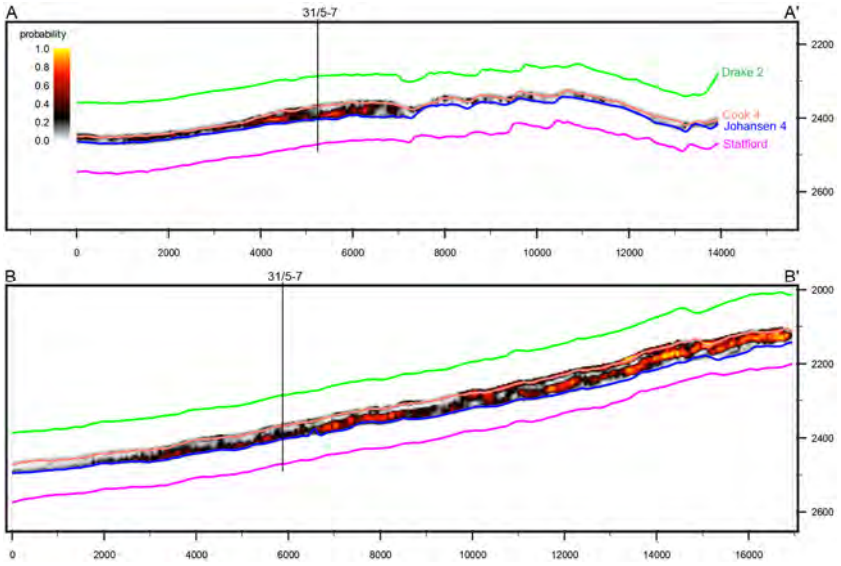

Figure 10: Posterior probability of Cook sandstone along sections A-A' and B-B'. Solid colored lines correspond to interpreted horizons.

In cross-section A-A' towards the east, the posterior probability of Cook sandstone becomes close to zero, which could indicate that it pinches out or that it is thinner than the seismic tuning thickness. Corresponding MCMC simulations giving the expected number of layers of the Cook sandstone is plotted in Figure 11. It clearly shows that the Cook sandstone diminish eastwards from well 31/5-7.

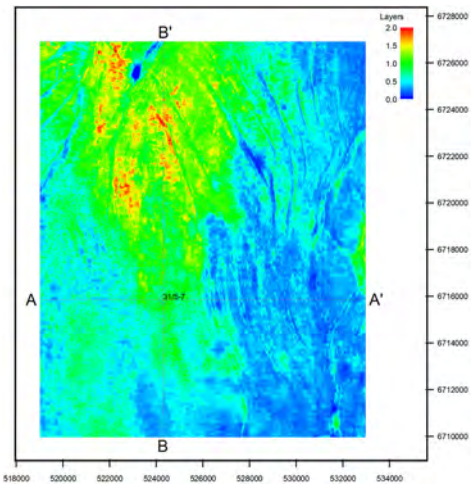

Figure 11: Expected number of layers of Cook sandstone.

6.3 P90, P50, and P10 thickness maps

From the cumulative thickness distributions of the MCMC simulations, we can make low, median, and high thickness estimates of the Cook and Johansen sandstones. Figures 12 and 13 show the P90 (low), P50 (median), and P10 (high) in the inversion area for Johansen and Cook sandstones, respectively. Here P90 means that 90% of the realizations are thicker than the estimate, and P10 means the 10% thickest realizations. Since the distributions are not symmetric around the mean value, the median thickness in Figure 12b) is slightly different from the expected (mean) thickness in Figure 8.

From the thickness maps, we observed that the Cook sandstone is thickest towards north and west in the inversion area with a median thickness of about 30 ms. The thickness of the Johansen sandstone is higher, with peaks at about 80 ms east of the well 31/5-7. It is interesting to observe the NNE to SSW boundary between thicker and thinner sands in Figure 12a.

Future work should focus on investigating the robustness of the inversion with respect to variability in the prior model. The classification into facies that was suggested in Figures 4 and 5 should be refined by more detailed rock physics analysis. Hopefully, it could give a better distinction between the Cook sandstone and the Dunlin shale and improve the classification in the Statfjord formation. Finally, the result of the inversion should be confirmed by the geological interpretation of well 31/5-7.

7. Conclusions

We have inverted the seismic data around the prosed CO_2 injection well 31/5-7 of the Aurora prospect. The inversion was done using the probabilistic inversion methodology developed at the Norwegian Computing Center. The inversion estimates the probability for Cook and Johansen sandstones encased in the Early Jurassic Dunlin group's shale. MCMC simulations on the inverted result provide estimates of sand thicknesses and expected layering.

The Johansen sandstone is abundant in the inversion area and thickest to the east, with an estimated total thickness above 60 ms. Towards north and west, the sandstone is thinner and seems to split into an upper and lower unit with potentially a thin shale layer in between.

The Cook sandstone is generally much thinner than the Johansen sandstone, and it pinches out towards the east. The estimation of the expected number of layers, that is, the vertical sum of probability of presence may be used to identify the boundary where it pinches out.

The presented methodology defines a functional workflow for quantifying the probability of presence and thickness uncertainty of the reservoir sands. Such results are useful input for future CO_2 injection strategies and migration predictions.

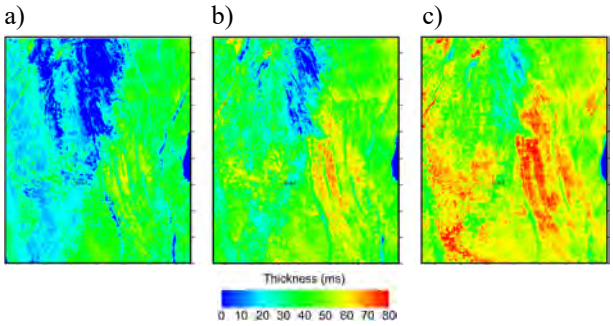

Figure 12: Thickness estimates of Johansen sandstone corresponding to a) P90, b) P50, and c) P10.

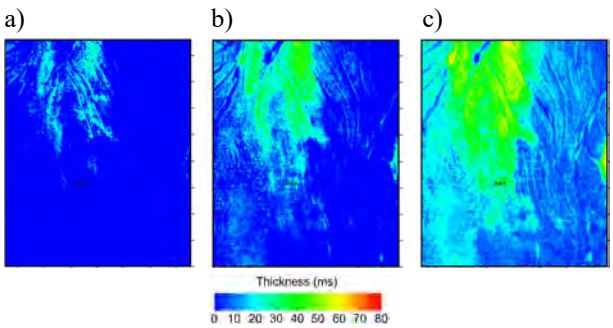

Figure 13: Thickness estimates of Cook sandstone corresponding to a) P90, b) P50, and c) P10.

Acknowledgments

We thank Gassnova for permission to use the seismic data and the Norwegian Petroleum Directorate for providing access to well data through the Norwegian National Data Repository for Petroleum data (DISKOS). We also thank the sponsors of the GIG consortium, AkerBP, ConocoPhillips, Equinor, Lundin, Total, Vår Energi, and Wintershall Dea, for financing the development of the algorithm used in this paper. Finally, we thank D. Barker at the Norwegian Computing Center for assistance when generating thickness histograms and

J. Rahman at UiO for seismic interpretation of the key horizons.

This work has been funded by the Norwegian Computing Center and The Norwegian Research Council through the CLIMIT program, project no. 280472 (OASIS) with financial support from Equinor and Total.

References

[1] Larsen, A. L., Ulvmoen, M., Omre, H., Buland, A. (2006). Bayesian lithology/fluid prediction and simulation on the basis of a Markov-chain prior model, Geophysics, **71**, R69–R78.

[2] Grana, D., & Rossa, E. D. (2010). Probabilistic petrophysical-properties estimation integrating statistical rock physics with seismic inversion, Geophysics, **75**, O21–O37.

[3] Kemper, M., & Gunning, J. (2014). Joint impedance and facies inversion—Seismic inversion redefined, First Break, **32**, 89–95.

[4] Connolly, P., & Hughes, M. (2016). Stochastic inversion by matching to large numbers of pseudo-wells, Geophysics, **81**, M7–M22.

[5] Nawaz, M.A., & Curtis, A. (2018). Variational Bayesian inversion (VBI) of quasi-localized seismic attributes for the spatial distribution of geological facies, Geophysics. J. Int., **214**, 845–875.

[6] Kolbjørnsen, O., Buland, A., Hauge, R., Røe, R., Ndingwan, A.O., Aker, E. (2020). Bayesian seismic inversion for stratigraphic horizon, lithology, and fluid prediction, Geophysics, **85**, R207-R221.

[7] Aki, K., & Richards, P.G. (1980). Quantitative seismology, W. H. Freeman. and Co.

[8] Krumbein, W.C., & Dacey, M.F. (1969). Markov chains and embedded Markov chains in geology: Mathematical Geology, **1**, 79–96.

[9] Ulvmoen, M., & Omre, H. (2010). Improved resolution in Bayesian lithology/fluid inversion from prestack seismic data and well observations – Part 1: Methodology: Geophysics, **75**, R21–R35.

[10] Ulvmoen, M., Omre, H., Buland, A. (2010). Improved resolution in Bayesian lithology/fluid inversion from prestack seismic data and well observations – Part 2: Real case study: Geophysics, **75**, B73–B82.

[11] Rimstad, K. & Omre, H. (2010). Impact of rock-physics depth trends and Markov random fields on hierarchical Bayesian lithology/fluid prediction: Geophysics, **75**, R93–R108.

[12] Gunning, J. & Sams, M. (2018) Joint facies and rock properties Bayesian amplitude-versus-offset inversion using Markov random fields: Geophysical Prospecting, **66**, 904–919.

[13] Steel, R., Ryseth, A. (1990). The Triassic – Early Jurassic succession in the northern North Sea: megasequence stratigraphy and intra-Triassic tectonics. Geological Society, London, Special Publications **55**, 139–168.

[14] Steel, R.J. (1993). Triassic – Jurassic megasequence stratigraphy in the Northern North Sea: rift to post-rift evolution, in: Geological Society, London, Petroleum Geology Conference Series. Geological Society of London, 299–315.

[15] Stewart, D.J., Schwander, M., Bolle, L. (1995). Jurassic depositional systems of the Horda Platform, Norwegian North Sea: Practical consequences of applying sequence stratigraphic models. Norwegian Petroleum Society Special Publications, 291–323.

[16] Husmo, T., Hamar, G.P., Høiland, O., Johannesen, E.P., Rømuld, A., Spencer, A.M., Titterton, R. (2003). Lower and Middle Jurassic. In: Evans, D., Graham, C., Armour, A., Bathurst, P. (Eds.), The Millennium Atlas: Petroleum Geology of the Central and Northern North Sea. The Geological Society, London, UK, 129-155.

[17] Partington, M.A., Copestake, P., Mitchener, B.C., Underhill, J.R. (1993). Biostratigraphic calibration of genetic stratigraphic sequences in the Jurassic-lowermost Cretaceous (Hettangian to Ryazanian) of the North Sea and adjacent areas. In: Parker, J.R. (Ed.), Petroleum Geology of Northwest Europe: Proceedings 4th Conference London (1992). Geological Society of London, UK, 371-386.

[18] Vollset, J. & Doré, A. G. (eds.) 1984: A revised Triassic and Jurassic lithostratigraphic nomenclature for the Norwegian North Sea. NPD-Bulletin No. 3.

[19] Norwegian Petroleum Directorate Fact-pages (2021), URL https://factpages.npd.no/ (accessed 11.01.21).

[20] Sundal, A., Nystuen, J.P., Dypvik, H., Miri, R., Aagaard, P. (2013). Effects of geological heterogeneity on CO2 distribution and migration–a case study from the Johansen Formation, Norway. Energy Procedia **37**, 5046–5054.

[21] Buland, A., & Omre, H. (2003). Bayesian linearized AVO inversion, Geophysics, **68**, 185–198.

[22] Sundal, A., Nystuen, J.P., Rørvik, K-L., Dypvik, H., Aagaard, P. (2016). The Lower Jurassic Johansen Formation, northern North Sea – Depositional model and reservoir characterization for CO_2 storage, Marine and Petrol. Geol. **77**, 1376-1401.